A Continuity Equation Based Optical Flow Method for Cardiac Motion Correction in 3D PET Data

Mohammad Dawood[1,2★], Christoph Brune[2], Xiaoyi Jiang[2], Florian Büther[1], Martin Burger[2], Otmar Schober[3], Michael Schäfers[1,3], and Klaus P Schäfers[1]

[1] European Institute for Molecular Imaging, University of Münster,
Mendelstr. 11, 48149 Münster, Germany
[2] Department of Mathematics and Computer Science, University of Münster,
Einsteinstr. 62, 48149 Münster, Germany
[3] Department of Nuclear Medicine, University Hospital Münster
Albert-Schweitzer-Str. 33, 48149 Münster, Germay

Abstract. Cardiac Motion artifacts in PET are a well known problem. The heart undergoes two types of motion, the motion due to respiratory displacement and the motion due to cardiac contraction. These movements lead to blurring of data and to inaccuracies in the quantification. In this study a continuity equation based optical flow method is presented and results on 3D PET patient datasets for cardiac motion correction are presented. The method was evaluated with respect to three criteria: correlation between the images, myocardial thickness and the blood pool activity curves. The results showed that the method was successful in motion correcting the data with high precision.

Keywords: Motion correction, Optical Flow, PET, CT, Mass Conservation

1 Introduction

PET (Positron Emission Tomography) is one method of acquiring metabolic information in patient studies, e.g. to visualize and quantify glucose metabolism in the body. To achieve this, a radioactive substance is injected in the patient body prior to image acquisition. The radioactive isotope decays with time and emits radiation which can be detected in specially built scanners. The distribution of the radioactivity in the body can thus be visualized and gives information on the metabolism. In PET, β^+ radioactive molecules are used for this purpose. These molecules emit positrons which collide with electrons and produce two gamma quanta which fly away from each other in opposite directions. The gamma quanta can now be detected in the scintillation detectors of the PET scanner. Using specialized reconstruction methods the activity distribution can thus be reconstructed [1].

★ dawood@uni-muenster.de

As this process of image acquisition requires a relatively long period of time, typically several minutes, the motion of the heart due to respiration and due to the cardiac contraction blurs the images. Image blur may cause wrong staging [2], inaccurate localization [4] and wrong quantification [5] of lesions. Thus PET studies have to take this into account.

This problem is compounded further if computed tomography (CT) data is used for attenuation correction, as in the case of modern PET/CT scanners. The CT data represents a snapshot in comparison to the PET images and therefore, the PET data is not always in spatial correspondence with the CT data.

One method of avoiding this problem is to use respiratory and cardiac signals from the patient to divide the PET data into phases with respect to either or both signals [6]. This is called gating. However, gating leads to reduction of the amount of information per phase. To get the same amount of information the image acquisition time has to be proportionally extended or the amount of radioactivity has to be increased. The first option is costly whereas the second exposes the patients to increased radioactivity.

Most recent studies related to this problem estimate the motion on the high resolution and less noisy gated CT images [7],[8],[9]. But this comes at the cost of an increased exposure of the patient to x-rays, which should be avoided where possible.

Two important studies related to the correction for cardiac motion are [10] and [11]. In the first study optical flow is used for estimating the deformations in the images by modeling the myocardium as an elastic membrane. The second study combines the motion estimation of the first study with reconstruction in a single framework. However this study is confined to 2D images and deals with cardiac motion.

1.1   Aim

The aim of this study is to present a new method based on optical flow which can correct the PET images for cardiac motion and is also computationally simple enough to allow reasonable times for motion correction. The method is essentially different from the brightness consistency based optical flow methods [12],[16] as it is based on the continuity equation. This change in the basic model is necessary as brightness consistency is not given in cardiac gated PET data due to the partial volume effect (PVE).

The PVE is a result of the limited resolution of the scanners. All objects smaller than the scanner resolution limit can not be accurately delimited and therefore appear blurred. As the heart muscle contracts and expands during the cardiac cycle its thickness varies. In phases with thicker heart wall, the activity is better resolved and has a higher amplitude as compared to other phases where the activity is spread over a larger area. However, the total amount of the activity remains the same.

The presented method is thus applicable to gated cardiac PET data. It is evaluated on software phantom and real patient data.

2   Intensity and Mass Conserving Optical Flows

Optical flow methods estimate the motion between two image frames. As a voxel with intensity $I(x, y, z, t)$ moves between the two frames, its intensity is assumed to remain constant in intensity conserving optical flow methods. Therefore the following equation holds [16]:

$$I(x, y, z, t) = I(x + \delta x, y + \delta y, z + \delta z, t + \delta t) \tag{1}$$

Here x, y, z are the spatial 3D coordinates and t is the time. Assuming the movement to be small enough and with Taylor expansion we get:

$$I_x u + I_y v + I_z w = -I_t \ \text{ or}$$
$$\nabla I \cdot \mathbf{u} = -I_t \tag{2}$$

with u, v, w for the x, y and z components of the velocity or optical flow $\mathbf{u}$, and I_x, I_y, I_z, I_t for the derivatives of the intensity image I in corresponding directions, respectively time.

To find the optical flow from this equation with three unknowns, additional constraints are required. Smoothness in flow is one such constraint. The famous optical flow algorithm by Horn/Schunck [17] also uses this constraint. The optical flow is thus found using an iterative scheme, whereby an energy functional is minimized. This functional can be given as:

$$f = \min \int ((\nabla I \cdot \mathbf{u} + I_t)^2 + \alpha(|\nabla u|^2 + |\nabla v|^2 + |\nabla w|^2)) \mathrm{d}x \mathrm{d}y \mathrm{d}z \tag{3}$$

where larger values of α lead to a smoother flow. The minimization can be achieved by calculating the corresponding Euler-Lagrange equations.

Such methods have been applied to the problem of respiratory motion on 3D PET/CT data successfully [15].

The optical flow estimation presented so far is applicable to data where the intensity of the objects remains constant. However, in some cases this constraint does not hold true. Cardiac PET studies are one such example. As the resolution of the PET scanners is limited, the real radioactive intensity present in an object cannot be accurately located below the limit of resolution resulting in image blur. In case of the heart, the myocardium (the heart muscle) expands and becomes thin in the end-diastolic phase whereas it contracts and becomes thick in the end-systolic phase (see figure 1). Therefore, the intensity seen on PET images of the myocardium varies largely depending upon the heart phase under observation.

In the case of cardiac PET images, another approach is thus required. The here presented method is based upon the continuity equation, more precisely upon the conservation of mass. This law says that the mass in a closed system is conserved. If we substitute activity by mass, the law must still hold, as the total activity in the system remains same from systolic to diastolic phases of the heart. It is only blurred in the diastolic phase. It should be noted that our data is pre-corrected for the time dependent radioactive decay during the reconstruction process so that the decay itself plays no role for our considerations.
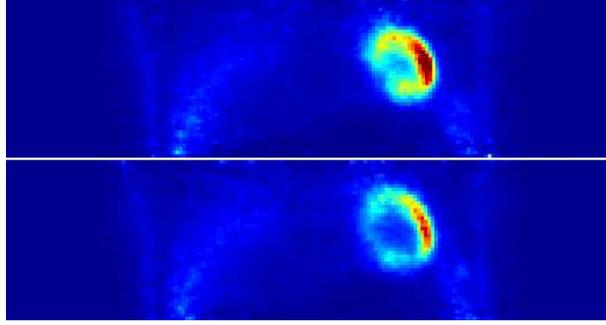
Fig. 1. Two phases from the cardiac cycle of the heart. Above: End-Systole, Below: End-Diastole. A coronal slice from the 3D PET image volume is shown. Images from an FDG study are shown here without attenuation correction.

The continuity equation for mass conservation is given as [13]:

$$\frac{\partial I}{\partial t} + div(I\mathbf{u}) = 0 \tag{4}$$

where I is the intensity value, $\mathbf{u} = (u, v, w)^T$ is the velocity vector i.e. the optical flow. Deviations from this eqution can be penalized by the following functional:

$$\int (\nabla I \cdot \mathbf{u} + I_t + I \cdot div(\mathbf{u}))^2 \mathrm{d}x\mathrm{d}y\mathrm{d}z \tag{5}$$

The derivative in time I_t can be calculated on discrete image volumes by using the difference: $I_2 - I_1$, where I_2 is the floating and I_1 is the target image volume. As with the intensity based optical flow, this is again an under-determined system of equations and therefore a smoothing term can be added to solve it. In the present study we used the same smoothing term as given in equation 3. The resulting optical flow functional is thus:
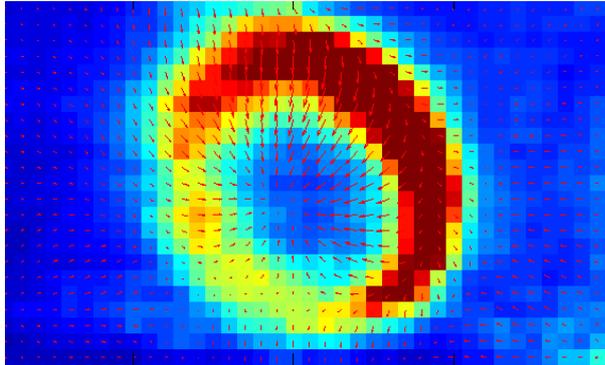
$$f = \mathrm{argmin}\left[\int_V D^2 dV + \alpha \int_V S dV\right] \tag{6}$$
$$\text{with}$$
$$D = div(I\mathbf{u}) + I_t, \quad S = |\nabla u|^2 + |\nabla v|^2 + |\nabla w|^2$$

The minimization of the equation (6) can be achieved by using the corresponding Euler-Lagrange equations. These are given by:

$$\begin{aligned} 0 &= D_x I + \alpha \Delta u \\ 0 &= D_y I + \alpha \Delta v \\ 0 &= D_z I + \alpha \Delta w \end{aligned} \tag{7}$$

Fig. 2. The optical flow calculated with the proposed method. A coronal slice is shown with superimposed vectors. Only two components of the flow are shown.

where D_x, D_y, D_z are the first derivatives of D in the corresponding directions. The weighting parameter α was set to about 0.05 based upon our previous experience with the data.

Once the optical flow is found (see Figure 2), the images have to be transformed to get the motion corrected data. The equation (4) can be used for this purpose. As the time derivative I_t was calculated as $I_2 - I_1$ and the flow $\mathbf{u}$ is now assumed to be known, the transformed image can be calculated as:

$$I_{2mc} = I_2 + div(I_2\mathbf{u}) \tag{8}$$

3   Software Phantom and Patient Data

To validate the methods, software phantom data was used. The NCAT software phantom by segars et al [14] provides a widely used tool for emission tomographic data simulation. The phantom data were produced for a cardiac cycle with 10 phases. The first gate was set to be end-diastolic and thus the end-systolic phase was gate number 5. The voxel size was 3.125 mm in each direction. Default parameters for the size and activity were used. The data was noise free and contained only minimal partial volume effects.

Fourteen patients with known coronary artery disease were included in this study. Patients were routinely referred to the [18]FDG PET scan for evaluation of myocardial viability prior to revascularization. A listmode dataset was acquired for 20 minutes, 1 hour post injection of [18]FDG (4 MBq/kg). To enhance FDG uptake in the heart, the patients underwent a hyperinsulinemic euglycemic clamp technique prior to and during the scan [18]. All patients received β-blockers to slow down and stabilize the heart rate during CT examination.

The Siemens Biograph Sensation 16 PET/CT scanner (Siemens Medical Solution) with a dedicated listmode research package was used in these studies.

This PET scanner has a spatial resolution of around 6 mm [19]. The cardiac signal for gating was acquired during the PET acquisition. The listmode file contains the coincidences along with the time of occurrence. This information together with the ECG information was used to sort the data into 10 cardiac phases. The data was then reconstructed without attenuation correction with the help of an expectation maximization algorithm [3]. In patient datasets, the end-diastolic phase was gate 3 and the end-systolic phase was gate number 9.

4   Results and Discussion

The performance of the proposed method was estimated with help of three criteria. These are 1) the correlation coefficient, 2) the myocardial thickness and 3) the left ventricular blood pool activity. The results of these experiments are given below in the corresponding subsections.

In all studies the diastolic phase was used as the target gate. It should be remembered that the cardiac cycle does not follow a linear pattern. This means that some phases are very close to each other and there are large differences among others.

4.1   Correlation Coefficient

The spatial correlation between the original and the motion corrected volumes was calculated between the target phase (end-diastolic) and all other phases before and after motion correction. To discard the influence of the stationary voxels, such as out of body pixels, a 40x40x40 voxels large volume of interest (VOI) was selected around the heart. The correlation coefficient was then calculated as:

$$cc = \frac{\sum_m \sum_n (A_{mn} - \bar{A})(B_{mn} - \bar{B})}{\sqrt{(\sum_m \sum_n (A_{mn} - \bar{A})^2)(\sum_m \sum_n (B_{mn} - \bar{B})^2)}} \tag{9}$$

where $\bar{A}$ and $\bar{B}$ are the means intensities of the respective volume.

The results for the software phantom are given in Table 1. The average correlation after motion correction is 99.86 as compared to 88.51 before the same. Besides high correlation, it is to be noted that the variation among the uncorrected data is far greater (min 80.25, std: 2.67) than after motion correction (min 99.81, std: 0.23). This shows that the algorithm effectively corrected the motion for all phases.

Phase	1	2	3	4	5	6	7	8	9	10	Avg
Before MC	100.0	94.53	92.99	86.65	81.73	80.25	80.75	82.22	90.88	95.08	88.51
After MC	100.0	99.87	99.87	99.85	99.83	99.81	99.82	99.83	99.87	99.87	99.86

Table 1. Results of the correlation analysis on software phantom dataset.

An overview of results on patient data can be seen in Figure 3. For better readability the results are given only for the correlation of the end-systolic with the target phase. Again, a high mean of 99.76 for all patients (min 99.54, std: 0.11) as compared to the original data (min 71.70, std: 5.84) was achieved.
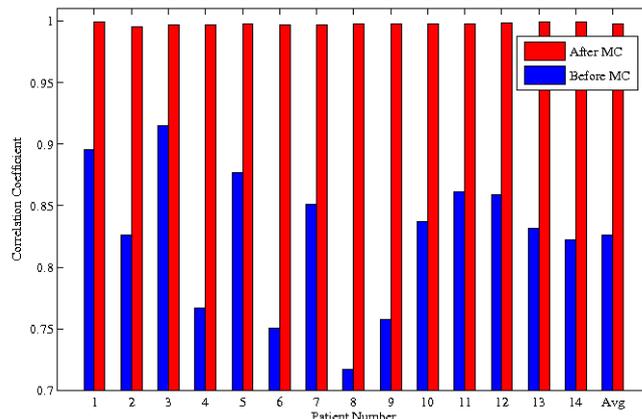
Fig. 3. Results of the correlation analysis on systolic phase of all patient datasets.

4.2 Myocardial Thickness

The thickness of the left ventricular wall increases from the end-diastolic to the end-systolic phase to pump blood into the arteries. As this variation follows the cardiac cycle, the wall thickness for all phases should correspond to that of the target phase after motion correction.

To calculate this measure, line profiles were taken across the left ventricular wall after manual reangulation of the heart. The distance between the ascending and descending flanks of the profile curve was taken as the width of the myocardial wall. For this the line profile was fitted with a gaussian curve and the FWHM of the fittgin function was used. To reduce the influence of noise, three consecutive slices were selected in the mid ventricular area and the average wall thickness calculated. As opposed to the correlation coefficient, this measure is more localized in nature.

The results on phantom data are given in Table 2 and show that the myocardial thickness is consistently (within 0.1 mm) similar to that of the target phase (to be recalled: voxel size was 3.125 mm^3). The standard deviation was reduced from 1.32 mm to 0.04 mm.

The results for patient data are given in Figure 4. The wall thickness was 17 mm on average in the end-systolic phase, which compared to 14 mm on average

Phase	1	2	3	4	5	6	7	8	9	10
Before MC	10.0	10.1	10.7	12.6	13.6	13.0	12.3	11.3	10.7	10.2
After MC	10.0	9.9	9.9	10.0	9.9	9.9	9.9	9.9	9.9	9.9

Table 2. Myocardial thickness [mm] on software phantom dataset.

for the end-diastolic phase. After motion correction the new transformed end-systolic phase also showed a wall thickness of 14 mm on average. The sum of squared differences between the wall thickness in end-systolic and end-diastolic phases was reduced from 133.9 to 2.5 after motion correction. The wall thickness appears larger than usual as attenuation correction was not performed.
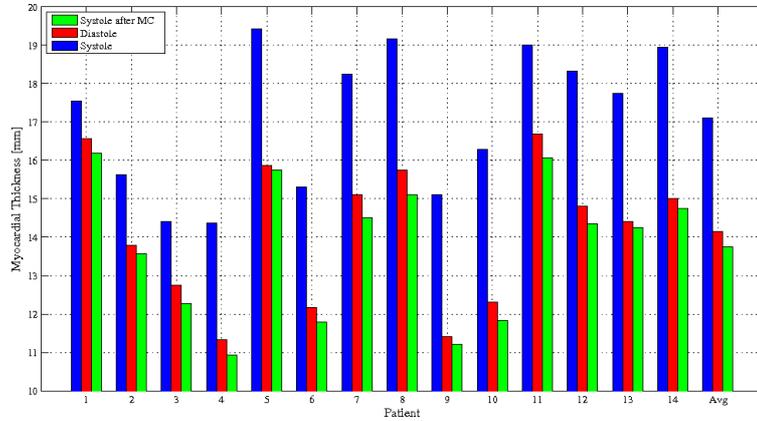

Fig. 4. Results of the myocardial thickness analysis on all patient datasets.

4.3   Mean Activity in Blood Pool

The third criterion to assess the performance was the mean activity in the blood pool in the left ventricle. Due to the PVE, activity radiates from the myocardium into the blood pool. In the end-systolic phase the blood pool is small, the ventricular walls closer to each other and accordingly there is a greater blurring effect as compared to the end-diastolic phase, when the blood pool is larger and the walls farther apart. After motion correction the blood activity values should be similar for all phases. For this analysis a 6x6x6 voxels large VOI was selected inside the left ventricle manually for each data set and the mean activity calculated in this VOI.

The results given in Figure 5 show that the activity in the blood pool becomes relatively independent of the cardiac phase after the proposed algorithm
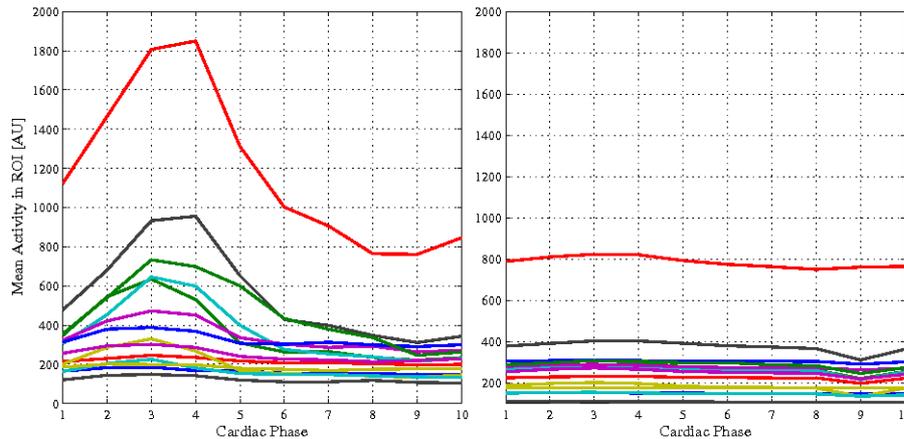
Fig. 5. Results of the mean activity in blood pool analysis among all patient datasets.

is applied. In the case of patient 10, the patient with the highest myocardial uptake on the Figure, the standard deviation of mean VOI activity among all cardiac phases was reduced from 409.5 to 26.5. The radiation into the blood increases with higher uptake in the myocardium. Consequently, the patients with high myocardial uptake show the largest variance among blood pool activities of the systolic and diastolic phases.

5   Conclusions

A continuity equation based optical flow method for cardiac PET data motion correction is presented. The method is able to correct the data despite partial volume effect. It was validated on patient and software phantom data. The results showed that the cardiac motion was corrected precisely.

References

1. S Vandenberghe, Y D'Asseler, R Van de Walle, T Kauppinen, M Koole, L Bouwens, K Van Laere, I Lemahieu, and RA Dierckx. Iterative reconstruction algorithms in nuclear medicine. *Comput Med Imaging Graph*, 25(2):105–111, 2001.
2. YE Erdi, SA Nehmeh, T Pan, A Pevsner, KE Rosenzweig, G Mageras, ED Yorke: H Schoder, W Hsiao, OD Squire, P Vernon, JB Ashman, H Mostafavi, SM Larson, and JL Humm. The CT motion quantitation of lung lesions and its impact on PET-measured SUVs. *J Nucl Med*, 45(8):1287–1292, Aug 2004.

3. LA Shepp and Y Vardi Maximum Likelihood Reconstruction for Emission Tomography. *IEEE Trans Med Imag*, 1(2):113–122, 1982.
4. MM Osman, C Cohade, Y Nakamoto, LT Marshall, JP Leal, and RL Wahl: Clinically significant inaccurate localization of lesions with PET/CT: frequency in 300 patients. *J Nucl Med*, 44(2):240–243, Feb 2003.
5. Y Nakamoto, BB Chin, C Cohade, M Osman, M Tatsumi, and RL Wahl: PET/CT: artifacts caused by bowel motion. *Nucl Med Commun*, 25(3):221–225, Mar 2004.
6. M Dawood, F Büther, N Lang, O Schober, and KP Schäfers. Respiratory gating in positron emission tomography: A quantitative comparision of different gating schemes. *Medical Physics*, 34:3067–3076, 2007.
7. F Qiao, T Pan, JW Clark, and OR Mawlawi. A motion-incorporated reconstruction method for gated PET studies. *Phys Med Biol*, 51(15):3769–3783, Aug 2006.
8. BA Mair, DR Gilland, and J Sun. Estimation of images and nonrigid deformations in gated emission CT. *IEEE Trans Med Imaging*, 25(9):1130–1144, Sep 2006.
9. F Lamare, MJL Carbayo, T Cresson, G Kontaxakis, A Santos, CCL Rest, AJ Reader, and D Visvikis: List-mode-based reconstruction for respiratory motion correction in PET using non-rigid body transformations. In *Phys Med Biol*, 52, pages 5187–5204, 2007.
10. GJ Klein, BW Reutter, and RH Huesman. Non-rigid summing of gated PET via optical flow. *IEEE Transactions on nuclear science*, 44(4):1509–1512, August 1997.
11. DR Gilland, BA Mair, JE Bowsher, and RJ Jaszczak. Simultaneous reconstruction and motion estimation for gated cardiac ECT. *IEEE Transactions on nuclear science*, 49(5):2344–2349, October 2002.
12. M Dawood, F Büther, X Jiang, and KP Schäfers. Respiratory Motion Correction in 3D PET Data with Advanced Optical Flow Algorithms. *IEEE Trans Med Imaging*, 27(8):1164-75, 2008.
13. T Corpetti, D Heitz, G Arroyo, E Mémin and A Santa-Cruz. Fluid experimental flow estimation based on an optical-flow scheme. *Experiments in Fluids*, 40:80–97, 2006.
14. WP Segars. Development and application of the new dynamic NURBS-based cardiac-torso (NCAT) phantom, in Biomedical Engineering. *Dissertation, University of North Carolina*, 2001.
15. M Dawood, N Lang, X Jiang, and KP Schäfers. Lung motion correction on respiratory gated 3-D PET/CT images. *IEEE Trans Med Imaging*, 25(4):476–485, Apr 2006.
16. A Bruhn, J Weickert, and C Schnörr. Lucas/Kanade meets Horn/Schunck: Combining local and global optic flow methods. *International Journal of Computer Vision*, 61(3):211–231, 2005.
17. B Horn, and B Schunck. Determining optical flow. *Artificial Intelligence*, 17:185–203, 1981.
18. GD Vitale, RA deKemp, TD Ruddy, K Williams, and RS Beanlands. Myocardial glucose utilization and optimization of (18)F-FDG PET imaging in patients with non-insulin-dependent diabetes mellitus, coronary artery disease, and left ventricular dysfunction. *J Nucl Med*, 42(12):1730–1736, 2001.
19. YE Erdi, SA Nehmeh, T Mulnix, JL Humm, and CC Watson: PET performance measurements for an LSO-based combined PET/CT scanner using the national electrical manufacturers association nu 2-2001 standard. *J Nucl Med*, 45(5):813–821, May 2004.